Chinese Journal of Polymer Science Vol. 34, No. 8, (2016), 1021–1031

Chinese Journal of Polymer Science

The Effect of Polymer-Substrate Interaction on the Nucleation Property: Comparing Study of Graphene and Hexagonal Boron Nitride Nanosheets*

Yi-ren Tang[a], Ting Li[a], Hai-mu Ye[b], Jun Xu[a**] and Bao-hua Guo[a**]

[a] *Advanced Materials Laboratory of Ministry of Education, Department of Chemical Engineering, Tsinghua University, Beijing 100084, China*

[b] *Department of Materials Science and Engineering, China University of Petroleum, Beijing 102249, China*

Abstract Hexagonal boron nitride nanosheets (BNNSs) can work as a more efficient nucleating agent for two polyesters compared to graphene. Studies on the crystallization and dewetting processes of two polyesters, poly(butylene succinate) and poly(butylene adipate), on the two substrate surfaces prove that the interaction between BNNSs and the polyesters is stronger than that between graphene and the polyesters. This strong interaction induces the pre-ordered conformation of molten PBA which has been identified by the *in situ* FTIR spectra. Thus BNNSs possess higher nucleation property than graphene. Finally, a new polymer-substrate interaction induced nucleation mechanism was proposed to explain the nucleation efficiency difference between graphene and BNNSs.

Keywords: Hexagonal boron nitride nanosheets; Graphene; Crystallization; Dewetting; Interaction.

Electronic Supplementary Material Supplementary material is available in the online version of this article at http://dx.doi.org/10.1007/s10118-016-1816-2.

INTRODUCTION

Nucleating agent is an important research topic for semi-crystalline polymers since it regulates the crystallization rate[1–3], the crystallization structure[4–6], transparency[7, 8] and the mechanical properties[9] of polymers. So far, two interpretations have been recognized as the mechanism of nucleating agent. One is the chemical nucleation, which was established by Mercier and Nield[10]. The other one is the epitaxial nucleation of polymer on external substrate, which was initiated by Lotz and Wittman[11]. A two dimensional lattice matching of the polymer matrix and the nucleating agent is necessary for epitaxial nucleation, and the limit range of lattice mismatch should be less than 15%[12]. The epitaxial nucleation can explain the working mechanism of a majority of nucleating agents, especially in polyethylene, polypropylene, polyesters, *etc*[13–16].

Graphene, a novel two-dimensional nanomaterial, has created the greatest sensation due to its fascinating properties in thermal conductivity, electrical conductivity, and mechanical properties[17–19]. An obvious application of graphene is in the field of polymer nanocomposites. In some cases, graphene or its derivatives possess heterogeneous nucleating property. Li *et al*.[20] used controlled solution crystallization method to induce polyethylene (PE) epitaxial growth on reduced graphene oxide (RGO). From SAED results, they found an

* This work was financially supported by the National Basic Research Program of China (No. 2014CB932202), the National Natural Science Foundation of China (Nos. 51473085 and 21374054) and the Sino-German Center for Research Promotion.
** Corresponding authors: Jun Xu (徐军), E-mail: jun-xu@mail.tsinghua.edu.cn
Bao-hua Guo (郭宝华), E-mail: bhguo@mail.tsinghua.edu.cn
Received February 14, 2016; Revised March 14, 2016; Accepted March 17, 2016
doi: 10.1007/s10118-016-1816-2

epitaxial relation of (0001) <2-1-10> RGO// (110) <001> PE. Gu *et al.*[21] also observed that poly(ε-caprolactone) (PCL) chain epitaxially grew along the <2-1-10> direction of the RGO (0001) plane, forming edge-on lamellae by using the same method as Li. Sano *et al.*[22] reported that nylon-6 could epitaxially crystallize on highly oriented pyrolytic graphite (HOPG) by an anionic ring-opening polymerization in HOPG dimethoxyethane solution. The interchain hydrogen bonding N—H···O=C assists polymer chain lie in the <10-10> direction of HOPG. However, the evidence of lattice matching or crystal plane overlap only exists in these novel preparation methods. The traditional solution mixing or melt blending method widely used in academic and industry cannot provide the proof of crystal matching even if graphene works as a nucleating agent[23–25]. BNNSs also possess the same hexagonal crystal lattice as graphene. The lattice parameter of BNNSs is a = 0.248 nm, which is approximate to that of graphene (a = 0.247 nm)[26]. Based on the epitaxial nucleation mechanism, BNNSs and graphene should exhibit the similar nucleation capability as nucleating agents. However, we found that the nucleation efficiency of BNNSs is much higher than that of graphene, especially in the polyesters, poly(butylene succinate) (PBS) and poly(butylene adipate) (PBA). The crystallization temperature (T_c) of PBS during cooling from melt increased from 76.2 °C to 91.9 °C only by adding 0.3 wt% BNNSs[27]. In contrast, after *in situ* polymerization blending or solution blending with GO, the T_c of PBS only rised from 67.5 °C to 73.6 °C or from 69.7 °C to 75.7 °C[28, 29]. When PBA was mixed with BNNSs or GO/RGO, the similar results were also obtained[30]. The crystallization behaviors of PBS nanocomposites and PBA nanocomposites prepared in our lab are summarized in Fig. 1. From the DSC cooling results, BNNSs exhibit much better nucleation property by increasing the crystallization peak temperature of PBS and PBA prominently. From those results, we speculate that there may exist other nucleation mechanism to explain the different nucleation efficiencies of graphene and BNNSs. Our latest report found that BNNSs could induce the formation of α-form nuclei of PBA due to the "melt memory" effect[30]. The strong interface interaction that anchors the PBA molecular chains at the surface of BNNSs was responsible for the "melt memory" effect. However, the polymer and 2D-material composite system is not suitable for the further research of interfacial interaction between them. Herein we study the crystallization and dewetting process of two polyester thin films on BNNSs and graphene substrates and focus on the interfacial interaction between them to clarify the nucleation mechanism.

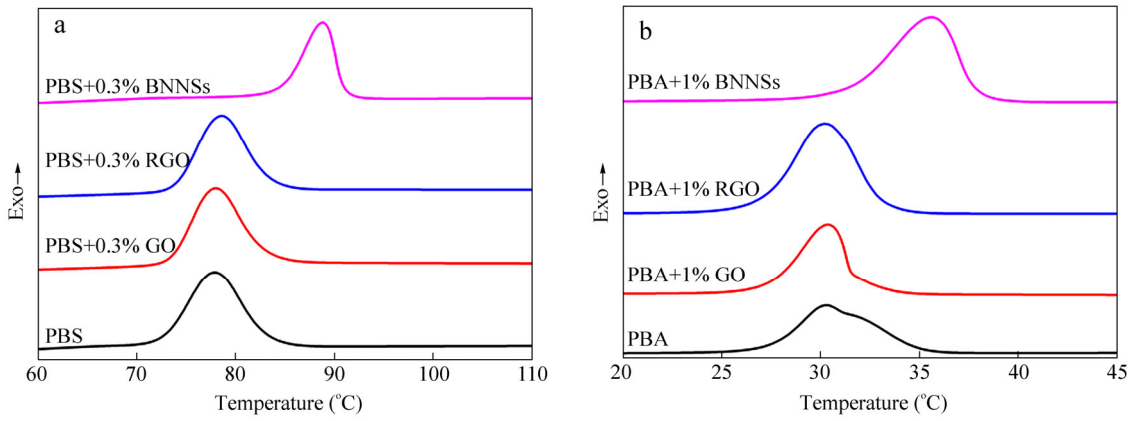

Fig. 1 DSC cooling curves of (a) PBS and PBS nanocomposites, (b) PBA and PBA nanocomposites from molten state at a rate of 10 K/min

EXPERIMENTAL

Materials and Sample Preparation

Poly(butylene succinate) (PBS) (melt index = 10 g/10min, 190 °C/2.16 kg), poly(butylene adipate) (M_w = 1.2 × 10^4 g/mol) were purchased from Sigma-Aldrich (Shanghai) Trading Co., Ltd. Atactic polystyrene (M_w = 1.25 × 10^5–2.5 × 10^5 g/mol) was purchased from Alfa-Aesar (Shanghai) Trading Co., Ltd. Multilayer hexagonal

boron nitride nanosheets (BNNSs) and graphene films were obtained from XF NANO (Nanjing) Materials Tech Co., Ltd. Graphene oxide (GO) was synthesized according to a modified Hummers method[31]. Hydroiodic acid was used to prepare reduced graphene oxide (RGO)[32].

To compare with the nucleating efficiency of BNNSs in our previous reports[27, 30], the additive weight percentages of GO and RGO were chosen as 0.3 wt% in PBS matrix and 1 wt% in PBA matrix. The co-solution method was utilized to prepare the nanocomposites of PBA or PBS/GO or RGO according to Ref. [4]. GO and RGO coated silicon wafer sheets for polarized optical microscopy (POM) observation were prepared by drop-casting their finely dispersed solution directly. The thickness of the GO and RGO films is 20–50 nm. The PS/toluene (2 wt%) solution was spin-coated on the *h*-BN substrates at 3000 r/min, resulting in a film with thickness of 30 nm.

Equipment and Characterization Techniques

A differential scanning calorimeter (Shimadzu DSC-60) was used to characterize the crystallization behaviors of the samples under a nitrogen atmosphere. The crystallization and melting temperatures of the samples were taken from the exothermal and endothermic peaks, respectively, at a cooling or heating rate of 10 K/min.

A Leica polarized optical microscope (DM2500P) was used to obtain the crystal morphology and the spherulitic radial growth rates (G) of PBA and the temperature was controlled by a Linkam THMS600 hot stage. The samples with thickness of 200 nm were prepared by drop-casting PBA/chloroform solution (10 mg/mL) on the glass (standard sample), *h*-BN, GO, RGO, and *a*-PS surface. The dewetting rate of PBS thin films (100 nm) were tested at 120 °C on graphene surfaces and 150 °C on BNNSs surfaces.

Wide-angle X-ray diffraction (WAXD) analysis was carried out at room temperature using a Rigaku D/max2550HB+/PCX-ray diffractometer with Cu Kα radiation. The isothermally crystallized samples (POM samples) were prepared by first anneal at 80 °C for 3 min at a hot stage and quickly transferred to the Linkam THMS600 hot stage at designated temperatures until the crystallization process finished.

Atom force microscopy (Shimadzu, 9700-J3) was utilized to characterize the surface morphology of PBA (POM samples) thin film and contact angle of PBS annealled thin film in tapping mode. The latter with thickness of 30 nm is prepared by spin-coating PBS/chloroform solution (5 mg/mL) on BNNSs and graphene surface at 3000 r/min. In order to obtain spherical droplets for the measurement of contact angle, PBS thin films were annealled at 130 °C for 6 h under the protection of nitrogen.

In situ Fourie transformation infrared (FTIR) spectra were collected by a Bruker Hyperion FTIR spectrometer with Grazing incident mode. PBA films with thickness of 200 nm on glass and BNNSs were used directly.

Surface tension of PBS was obtained by a contact angle analyser (Harke, SPACX1) *via* Owen method[33]. Two different solutions were used to measure the contact angle on PBS film at different temperatures. Then the surface tension of PBS could be calculated by the software of contact angle analyser with the data of contact angle.

RESULTS AND DISCUSSION

Comparison Study of Surface Nucleation

Firstly, the nucleation efficiency of different 2D-material substrates for PBA thin films was investigated. Figure 2 shows the nucleation induction time (t_I) and spherulite growth rate (G) of PBA thin films (200 nm) isothermally crystallized on different substrate surfaces. Considering that the oxygenic functional groups will affect the natural properties of graphene and PBA shows the similar t_I and G on graphene oxide (GO) and RGO surfaces (Fig. S1), we only show the results of RGO surface. Although BNNSs surface increases the primary nucleation rate of PBA, the G of PBA decreases obviously. The result on the atactic polystyrene surface (20 nm) prepared by spin-coating on the BNNSs surface verifies that the direct contact interface between BNNSs and PBA is the decisive factor for the variation of t_I and G. Song *et al.*[34] also found the similar result that the primary nucleation and G showed the opposite change when poly(ethylene oxide) and polypropylene crystallized on the graphene surface. The mechanism will be discussed in the following part.

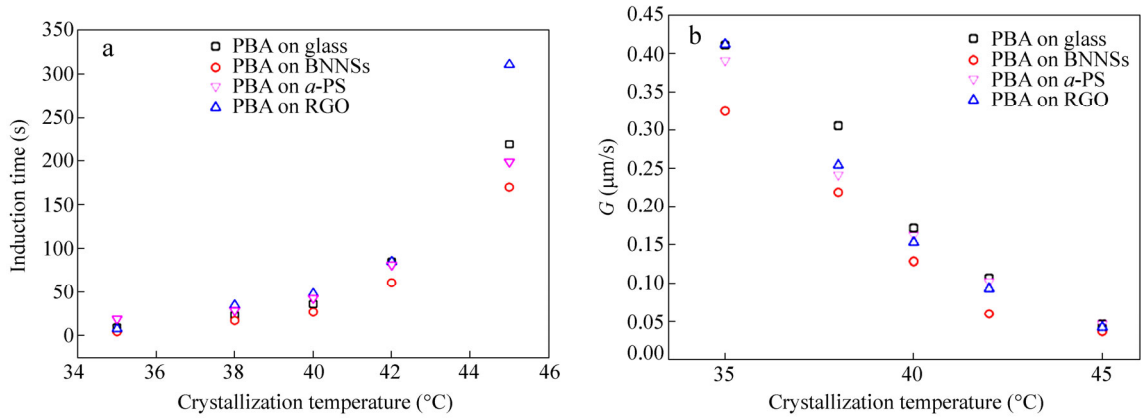

Fig. 2 (a) The nucleation induction time, and (b) G of PBA on different surfaces at various temperatures

It is interesting to find that the centers of PBA spherulites are different in Figs. 3(a) and 3(b). PBA can form many tiny primary nuclei in the white dotted circle quickly until coalescence and then grow radially as normal at 35 °C. The morphology of PBA on the graphene surface is similar with that on the glass surface and is not shown here. To clarify this phenomenon, AFM was used to reveal the fine structure of the samples. The orientation of PBA lamellar crystals on the glass is flat-on (Fig. 3c). However, bundle-like nuclei (white arrow) (Fig. 3d) are formed with an edge-on orientation in the white dotted circle (Fig. 3b). Outside the white circle, the spherulites grow the same as Fig. 3(c), with lamellar orientation turning to flat-on. Figure S2 shows the AFM patterns of PBA on the glass and BNNSs at various temperatures and the orientation of lamellar crystals is summarized in Table 1. It can be clearly seen that PBA film consists of flat-on and edge-on lamellae on BNNSs until α-form crystal disappears completely at the crystallization temperature of 0 °C. The WAXD results of PBA are shown in Fig. 4. BNNSs can change the optimal growth direction of PBA crystals, which makes the relative peak intensity of $\alpha(110)/\alpha(020)$ decrease due to its heterogeneous nucleation property[30]. While edge-on lamellae only appear at 30 °C when the mixed crystals of α-form and β-form PBA are formed on the glass. The lamellar orientation can be attributed to the combined effect of many plausible factors, such as temperature, film thickness, molecular weight, and substrate[35–37]. Sun *et al.*[38] found that the poly(vinylphenol) (PVPh) surface can induce the formation of poly(3-hydroxybutyrate) (PHB) crystal oriented with b-axis perpendicular to substrate due to stronger interaction between PVPh substrate and PHB molecular chain. Though the reasonable explanation for the edge-on lamellae of PBA on BNNSs surface is still unclear, there definitely exists strong interfacial interaction between PBA and BNNSs, which facilitates the formation of edge-on lamellae in the primary nucleation process. Koratkar *et al.*[39] reported that the wetting transparency of graphene originated from two-dimensional non-close-packed thin sheet geometry made the wetting behavior of graphene deviate from the bulk graphene and approach to its substrate until the thickness of graphene increased to a certain level. Thus the interaction force increasing with thicker BNNSs film obstructs the effect of substrate. We speculate that PBA chains possess stronger “melt memory” effect on the thicker area of the BNNSs film due to the more intensive adsorption force. The similar results that the interaction between polymer and substrate increased with the increase of substrate thickness had been reported previously[40, 41]. Due to the pre-ordered conformation in molten state, these chains can form primary nuclei quickly when they cooled from molten state. However, the stronger interaction not only assists chains to conquer primary nucleation energy barrier, but also decreases the secondary nucleation rate because the restricted mobility of chains leads to a slower diffusion rate. That’s the reason why the primary nucleation rate and G of PBA change with the opposite tendency on the BNNSs surface.

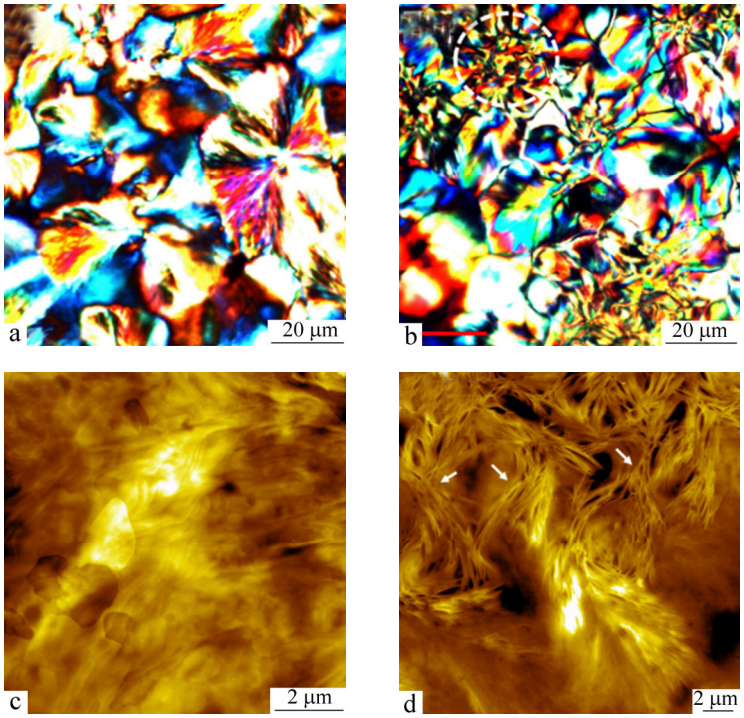

Fig. 3 Spherulitic morphologies of PBA (a) on the glass surface; and (b) on the BNNSs surface at 35 °C; (c) and (d) are the corresponding AFM height images of (a) and (b)

Table 1. Crystal form and lamellar orientation of isothermally crystalized PBA on different surface

Substrate	T_c = 35 °C		T_c = 30 °C		T_c = 20 °C		T_c = 10 °C		T_c = 0 °C	
	A	B	A	B	A	B	A	B	A	B
Glass	α	F	$\alpha+\beta$	E + F	β	F	β	F	β	F
BNNSs	α	E + F	$\alpha+\beta$	E + F	$\alpha+\beta$	E + F	$\alpha+\beta$	E + F	β	F

T_c is short for isothermal crystallization temperature; A stands for crystal form; B indicates lamellar orientation; Edge on and flat on orientation is abbreviated as E and F, respectively.

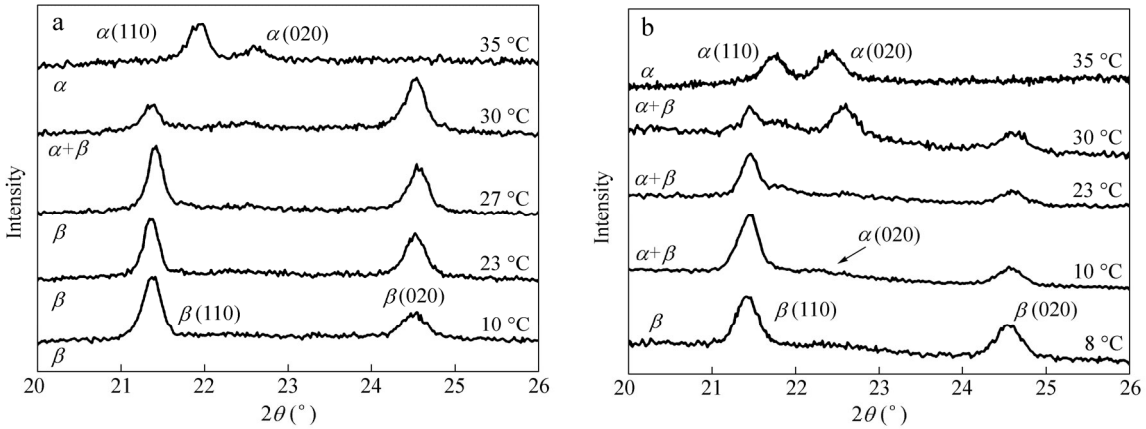

Fig. 4 WAXD patterns of isothermally crystalized PBA on (a) glass and (b) BNNSs at various crystallization temperatures

In order to prove that the strong interaction between BNNSs and PBA generates the pre-ordered conformation of PBA in the molten state, the *in situ* FTIR experiment was carried out. Figure 5 shows the FTIR spectra and their corresponding second derivatives of PBA molten films on the BNNSs surface and glass. PBA

films started crystallization at 45 °C, thus the spectra at the temperature of 50, 55, and 65 °C were only measured. Comparison of the second derivatives of Figs. 5(a) and 5(b) reveals that the 1479 cm^{-1} band appears in Fig. 5(a) at all the three temperatures. Several reports ascribed this absorption to the crystalline band of PBA[42, 43]. The 1459 cm^{-1} and 1448 cm^{-1} bands shift to higher wavenumber of 1463 cm^{-1} and 1452 cm^{-1}, respectively. Yan *et al.*[44] assigned 1463 cm^{-1} band to the CH_2 bending vibration in the PBA crystalline. Moreover, the carbonyl stretching vibration band at the 1734 cm^{-1} split into two bands at 1749 cm^{-1} and 1730 cm^{-1} when PBA is on the surface of BNNSs, as seen in Fig. 6. All these observations prove that the conformation of PBA chains on BNNSs is different from the random coil in the molten state on glass. Therefore, it is reasonable to suggest that the strong interaction between BNNSs substrate and PBA chains induces the pre-ordered conformation of PBA chains, which benefits the formation of primary nuclei.

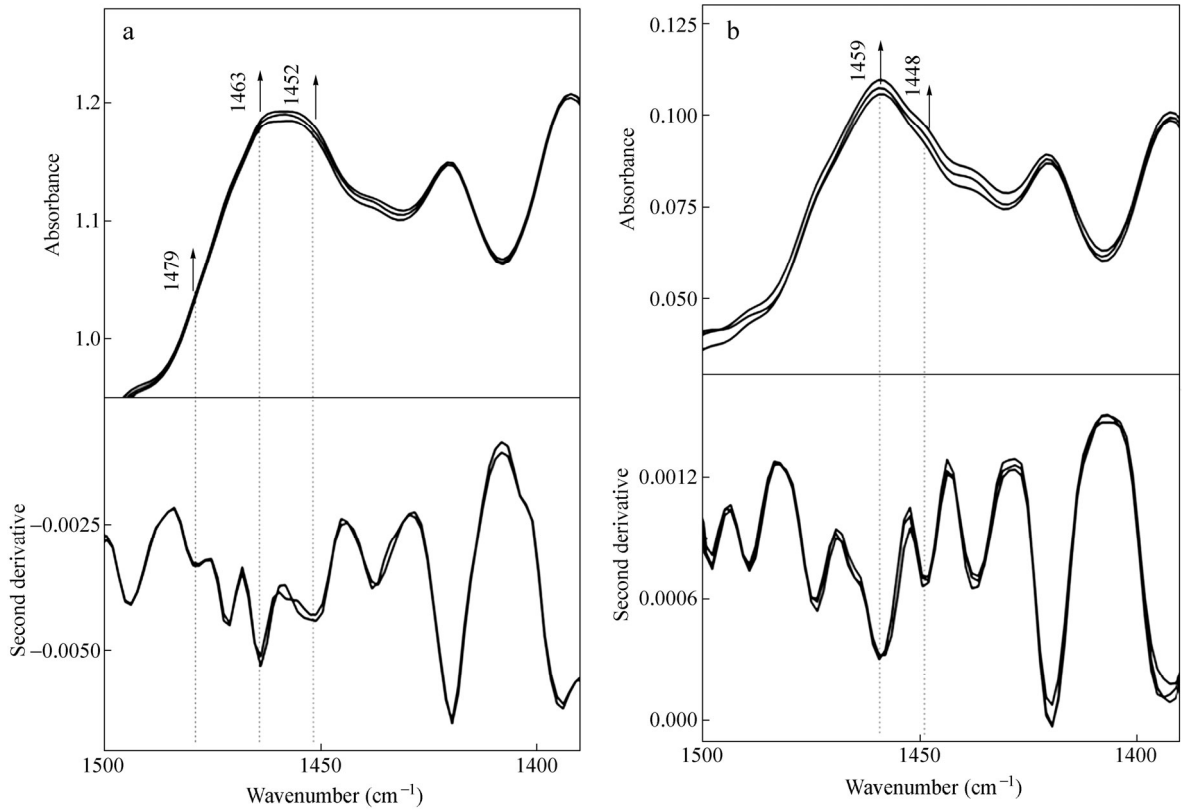

Fig. 5 Time-resolution FTIR spectra in the range of 1500–1390 cm^{-1} for PBA on (a) BNNSs, and (b) glass substrate during the cooling process from 65 °C to 55 and 50 °C
The half bottom is the corresponding second derivative of the spectra in the above graph. The arrow represents the decrease of temperature during cooling.

Comparison Study of Surface Dewetting

The dewetting behaviour of polymer thin films on solid substrates is dependent on their interaction[45, 46]. The stronger interaction can increase the frictional viscosity between the polymer film and substrate surface, thus decreasing the dewetting rate. The hole formation process during dewetting can be divided into three stages: the first stage ignores the frictional viscosity between liquid-solid interface, and the last stage is dominant by the slippage effect of polymer chain. Only in the second stage, the frictional viscosity between liquid-solid interface plays an important role[47]. Moreover, the hole diameter (R) grows linearly with time in the second stage instead of exponentially in the other stages. In order to obtain a slower dewetting rate, PBS is chosen instead of PBA. Figure 7 shows the distance of the hole edge of PBS thin films versus annealing time on different surfaces at the

second stage. The drop-casting RGO surface is too rough to obtain distinct graph. So the graphene film prepared by CVD method is used. Since the PBS melt film (100 nm) on graphene surface will rupture into small droplets immediately at 150 °C, we can only measure the dewetting rate at 120 °C. The dewetting rate of PBS on graphene surface at 120 °C is 1.3 μm/s. It is expected that the dewetting rate at 150 °C would be much larger. Comparing the different dewetting rates of PBS melt film on the graphene and BNNSs surfaces, we can conclude that the interaction between PBS and BNNSs surface is stronger than that between PBS and graphene.

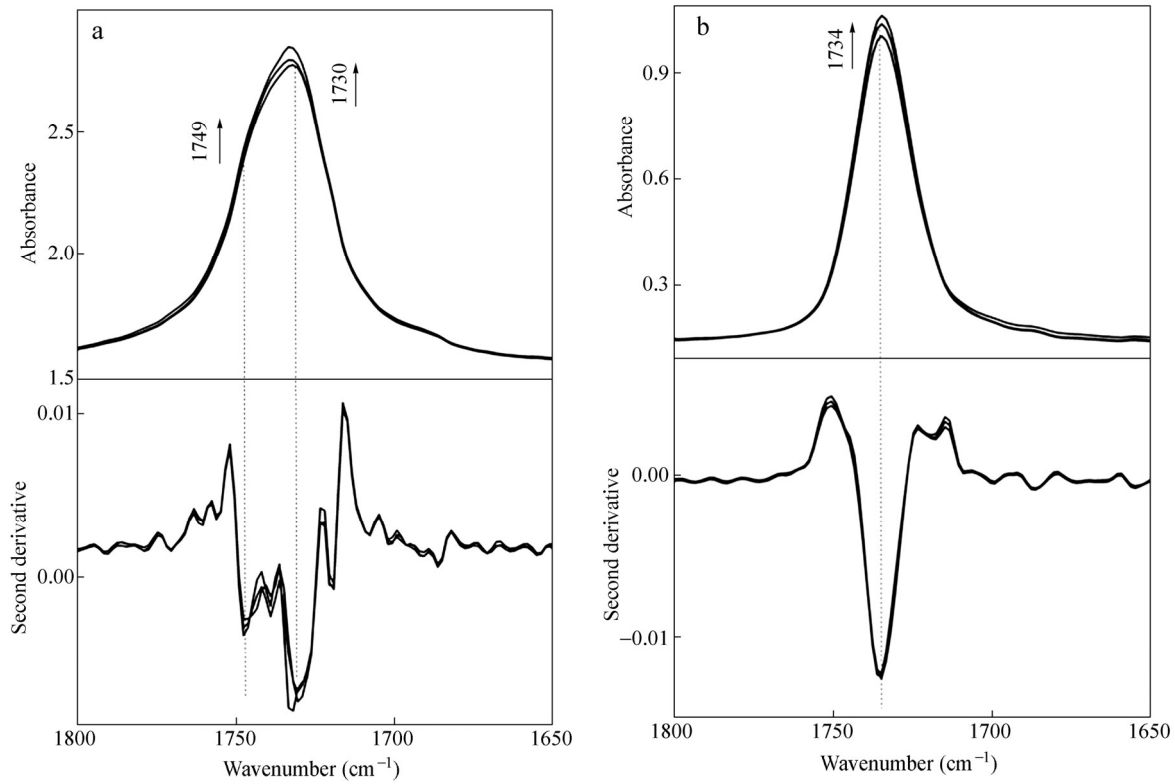

Fig. 6 Time-resolution FTIR spectra in the range of 1800–1650 cm^{-1} for PBA on (a) BNNSs, and (b) glass substrate during the cooling process from 65 °C to 55 and 50 °C (from bottom to top)
The half bottom is the corresponding second derivative spectra of the above graph. The arrow represents the decrease of temperature during cooling.

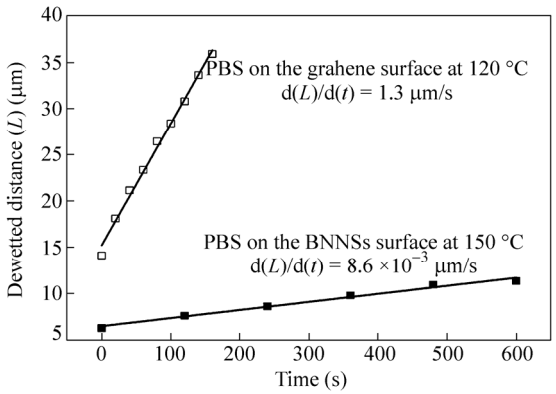

Fig. 7 Dewetted distance of PBS thin films versus time on the BNNSs and graphene surfaces

To further quantify the interfacial interaction between PBS and different substrates, AFM was used to measure the contact angle of microscopic droplets of PBS on BNNSs and graphene surface. In this study, ultrathin films of PBS (30 nm) on different surfaces were annealed at 130 °C for 6 h until the morphology remained stable. The contact angle in Fig. 8 is calculated by the following expression:

$$\tan(\frac{\theta}{2}) = \frac{H}{R} \tag{1}$$

The parameter H and R is the height and radius of a dewetted polymer droplet, respectively. To avoid the deviation, ten repeated measurements on the elaborately chosen circular droplet had been executed. Different droplet sizes give almost the similar contact angle values, which is in accordance with Shull's report[48]. The acquired contact angle of PBS melt on the BNNSs surface and graphene surface is (26.8 ± 3.9)° and (43.7 ± 4.5)°, respectively. The above results provide firm evidence that there exists stronger interaction between PBS and BNNSs. To calculate the surface energy of substrate, the well-known Young's relationship is used:

$$\sigma_s - \sigma_{sl} = \sigma_l \cos\theta \tag{2}$$

Here σ_l, σ_s, and θ are the surface tension of liquid, substrate, and contact angle. σ_{sl}, which can be deduced by Fowkes theory (Eq. 3), is the interfacial tension between the liquid and the substrate.

$$\sigma_{sl} = (\sigma_s^{1/2} - \sigma_l^{1/2})^2 \tag{3}$$

From Eqs. (2) and (3), we can obtain Eq. (4):

$$\sigma_s = \frac{\sigma_l}{4}(1+\cos\theta)^2 \tag{4}$$

The surface energy σ_l of PBS melt is 20.1 mN/m at 130 °C, which is calculated in our lab by Owen method. By substituting σ_l and θ into Eq. (4), the surface energies of BNNSs and graphene are determined to be 18.0 and 14.9 mN/m, respectively. The higher surface energy means that BNNSs is a more effective nucleating agent than graphene[49].

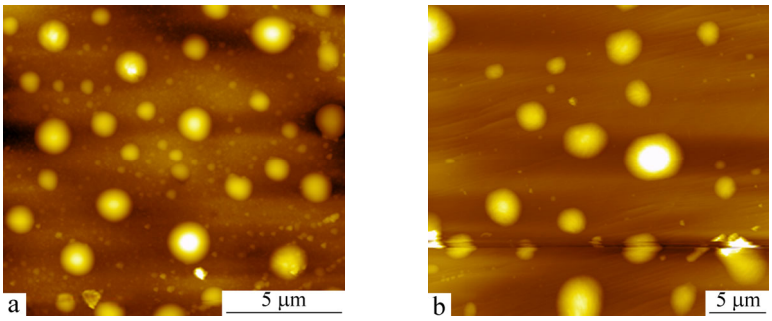

Fig. 8 AFM height image of PBS droplet on (a) BNNSs and (b) graphene

The strong interaction force between BNNSs and the studied polyester may originate from the van der Waals (vdW) and Coulomb interaction, which is due to the polar nature of B—N bonds. Chen *et al.*[50] proved that the binding energy of boron nitride nanotube (BNNT)-polar polymer caused by vdW and Coulomb interaction was much higher than that of CNT-polymer by MD simulation. Due to the similar chemical structure of BNNSs and BNNT, this result is also applicable to our case. However, graphene surface has weak interaction force with the polyester, which does not induce pre-ordered conformation of PBA and PBS molecular chains. Thus BNNSs have higher nucleating efficiency than RGO. On the contrary, the stronger interaction force between BNNSs and polyesters can induce a pre-ordered conformation of polymer chain in the molten state, which can nucleate faster under cooling. The crystallization process of polyesters on the two substrates has been

schematically represented in Fig. 9. We expect that the mechanism of interaction force induced nucleation exists not only in two-dimensional material, but also in other nano-materials. Although the tremendous surface area of two-dimensional materials made this mechanism more conspicuous than in other nucleating agents, some researchers still reported the similar results, which supported our nucleation mechanism. Carbon nanotube (CNT), a member of carbon family, is considered as seamless wrapping of graphene. Li *et al.*[51] reported that polyethylene and nylon 66 can form "nano hybrid shish-kebab" (NHSK) on the carbon nanotube by crystallization in solution. "Soft epitaxy" mechanism, in which the strict lattice matching between the CNT surface and polymer was not needed, was used to explain the nucleation mechanism. "Geometry confinement" provided by molecular curvature of fiber surface drives the polymer chain align on the fiber surface and then increases the nucleation rate of polymer. That's why CNT always exhibits higher nucleation efficiency than graphene[14, 52]. Moreover, Yan *et al.*[53] used the *in situ* FTIR spectrum to find that the highly oriented polyethylene (PE) could induce ordering of polycaprolactone (PCL) chains in its molten state *via* the strong interaction between them. It's noteworthy that CH-π interaction between PBA and carbon fiber can induce the pre-ordered conformation of PBA chains, as recently reported by Song *et al*[42]. Therefore, we can refresh the definition of "soft epitaxy" mechanism. The special interaction between nucleating agent and polymer, which is strong enough to induce pre-ordered conformation, can facilitate the crystallization of polymer without the requirement of matching of crystal lattice. Our result is important in the viewpoint of polymer crystallization and the practical application of biodegradable polyesters, because we have not only found an efficient nucleating agent, BNNSs, for several polyesters but also provided a method to screen other potential nucleating agents from inorganic 2D-materials and explain their nucleation mechanism.

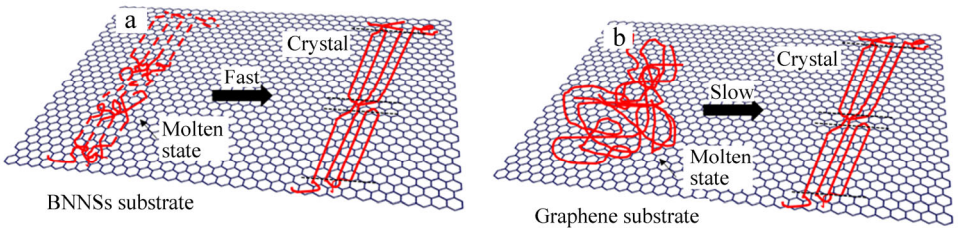

Fig. 9 Schematic diagram of the possible chain ordering process of polyester on two substrates

CONCLUSIONS

In summary, we have studied the surface nucleation of PBS and PBA on the BNNSs and graphene surfaces. BNNSs have more prominent nucleation efficiency than graphene. The lower dewetting rate and the smaller contact angle of PBS droplet on BNNSs surface reveal that the interaction force between BNNSs and the studied polymer is stronger than that between graphene and polymers. Furthermore, the strong interaction between BNNSs and PBA chains can induce the formation of α-form crystal accompanied by edge-on lamellar orientation. This interaction force may originate from the van der Waals (vdW) and Coulomb interaction, which anchors the polymer chains on the BNNSs surface. Those adsorbed polymer chains will have "memory effect" and possess pre-ordered conformation, which has been identified by the *in situ* FTIR spectrum in the molten state, thus they can nucleate faster during the cooling process. This polymer chain/substrate interfacial interaction that induced nucleation mechanism in the two-dimensional nucleating agent does not need strict epitaxial matching of crystal lattice.

REFERENCES

1 Chen, J.B., Xu, J.Z., Xu, H., Li, Z.M., Zhong, G.J. and Lei, J., Chinese J. Polym. Sci., 2015, 33(4): 576

2 Ye, H.M., Wang, R.D., Liu, J., Xu, J. and Guo, B.H., Macromolecules, 2012, 45: 5667

3 Pan, P.J., Yang, J.J., Shan, G.R., Bao, Y.Z., Weng, Z.X. and Inoue, Y., Macromol. Mater. Eng., 2012, 297: 670
4 Dong, T., Kai, W.H. and Inoue, Y., Macromolecules, 2007, 40: 8285
5 Leng, J.H., Liu, H., He, B.B., Yang, B., Chen, X. and Qin, Q.Q., Chinese J. Polym. Sci., 2013, 31(11): 1563
6 Sun, Y.J., Li, H.H., Huang, Y., Chen, E.Q., Zhao, L.F., Gan, Z.H. and Yan, S.K., Macromolecules, 2005, 38: 2739
7 Guo, X.J., Liu, H.Z., Zhang, J.W. and Huang, J.J., Ind. Eng. Chem. Res., 2014, 53: 4869
8 Lopes, A.C., Costa, C.M., Tavares, C.J., Neves, I.C. and Mendez, S.L., J. Phys. Chem. C., 2011, 115: 180762
9 Yang, B., Ni, H.K., Huang, J.J. and Luo, Y., Macromolecules, 2013, 47: 284
10 Legras, R., Mercier, J.P. and Nield, E., Nature, 1983, 304: 432
11 Wittmann, J.C. and Lotz, B., Prog. Polym. Sci., 1990, 15: 909
12 Wittmann, J.C. and Lotz, B., Polym. Sci., Polym. Phys. Ed., 1981, 19: 1837
13 Xin, R., Zhang, J., Sun, X.L., Li, H.H., Qiu, Z.B. and Yan, S.K., Adv. Polym. Sci., 2015, DOI: 10.1007/12_2015_329
14 Yan, S.K., Bonnet, M. and Petermann, J., Polymer, 2000, 41: 1139
15 Wu, Z.Q., Wang, G., Zhang, M.W., Wang, K. and Fu, Q., Soft Matter, 2016, 12: 594
16 Tang, Y.R., Gao, Y., Xu, J. and Guo, B.H., CrystEngComm, 2015, 17: 6467
17 Balandin, A.A., Ghosh, S., Bao, W.Z., Calizo, I., Teweldebrhan, D., Miao, F. and Lau, C.N., Nano Lett., 2008, 8: 902
18 Lee, C., Wei, X.D., Kysar, J.W. and Hone, J., Science, 2008, 321: 385
19 Zhang ,Y.B., Tan, Y.W., Stormer, H.L. and Kim, P., Nature, 2005, 438: 201
20 Cheng, S., Chen, X., Hsuan, Y.G. and Li, C.Y., Macromolecules, 2011, 45: 993
21 Wang, B.J., Zhang, Y.J., Zhang, J.Q., Li, H.Y., Chen, P., Wang, Z.B. and Gu, Q., Ind. Eng. Chem. Res., 2013, 52: 15824
22 Sano, M., Sasaki, D.Y. and Kunitake, T., Science, 1992, 258: 441
23 Jiang, Z.N. and Qiu, Z.B., RSC Adv., 2015, 5: 55486
24 Wang, G.S., Wei, Z.Y., Sang, L., Chen, G.Y., Zhang, W.X., Dong, X.F. and Qi, M., Chinese J. Polym. Sci., 2013, 31(8): 1148
25 Pang, H., Zhong, G.J., Xu, J.Z., Yan, D.X., Ji, X., Li, Z.M. and Chen, C., Chinese J. Polym. Sci., 2012, 30(6): 879
26 Nag, A., Raidongia, K., Hembram, K.P.S.S., Datta, R., Waghmare, U.V. and Rao, C.N.R., ACS Nano, 2010, 4: 1539
27 Tang, Y.R., Lin, D.W, Gao, Y., Xu, J. and Guo, B.H., Ind. Eng. Chem. Res., 2014, 53: 4689
28 Wang, X.W., Zhang, C.A., Wang, P.L., Zhao, J., Zhang, W. and Ji, J.H., Langmuir, 2012, 28: 7091
29 Du, X.C., Wang, Y.P., Huang, W.B., Yang, J.H. and Wang, Y., Colloid. Polym. Sci., 2015, 293: 389
30 Tang, Y.R., Xu, J. and Guo, B.H., Ind. Eng. Chem. Res., 2015, 54: 1832
31 Park, S.J., An, J.H., Piner, R.D., Jung, I., Yang, D.X., Velamakanni, A., Nguyen, S.T. and Ruoff, R.S., Chem. Mater., 2008, 20: 6592
32 Pei, S.F., Zhao, J.P., Du, J.H., Ren, W.C. and Cheng, H.M., Carbon, 2010, 48: 4466
33 Owen, M.J., J. Appl. Polym. Sci., 1988, 35: 895
34 Tong, Y., Lin, Y., Wang, S.D. and Song, M., Polymer, 2015, 73: 52
35 Frömsdorf, A., Woo, E.M., Lee, L.T., Chen, Y.F. and Fröster, S., Macromol. Rapid Commun., 2008, 29: 1322
36 Zhao, L.F., Wang, X.H., Li, L. and Gan, Z.H., Polymer, 2007, 48: 6152
37 Liu, J., Ye, H.M., Xu, J. and Guo, B.H., Polymer, 2011, 52: 4619
38 Sun, X.L., Chen, Z., Wang, F., Yan, S.K. and Takahashi, I., Macromolecules, 2013, 46: 1573
39 Rafiee, J., Mi, X., Gullapalli, H., Tomas, A.V., Yavari, F., Shi, Y.F., Ajayan, P.M. and Koratkar, N.A., Nat. Mater., 2012, 11: 217
40 Li, Q., Zhou, J.D., Chai, L.G., Memon, J., Ren, Z.J., Li, H.H., Sun, X.L. and Yan, S.K., Polym. Chem., 2014, 5: 4293
41 Zhou, J.D., Gan, H.Y., Ren, Z.J., Li, H.H., Zhang, J.M., Sun, X.L. and Yan, S.K., Polymer, 2014, 55: 5821
42 Song, Y.Y., Ye, H.M., Meng, X.Y., Zhou, Q. and Lu, G.W., RSC Adv, 2015, 5: 102384
43 Yang, J.J., Li, Z.G., Pan, P.J., Zhu, B., Dong, T. and Inoue, Y., J. Polym. Sci., Part B: Polym. Phys., 2009, 47: 1997
44 Yan, C., Zhang, Y., Hu, Y., Ozaki, Y., Shen, D.Y., Gan, Z.H., Yan, S.K. and Takahashi, I., J. Phys. Chem. B., 2008, 112: 3311
45 Hamieh, M., Akhrass, S.Al., Hamieh, T., Damman, P., Gabriele, S., Vilmin, T., Raphaël, E. and Reiter, G., J. Adhes., 2007, 83: 367

46 Han, X., Luo, C.Y., Dai, Y.Y. and Liu, H.L., J. Macromol. Sci. B., 2008, 47: 1050
47 Brochard-Wyart, F., Debregeas, G., Fondecave, R. and Martin, P., Macromolecules, 1997, 30: 1211
48 Vitt, E. and Shull, K.R., Macromolecules, 1995, 28: 6349
49 Schonhorn, H., Macromolecules, 1968, 1: 145
50 Chen, X.M., Zhang, L.Y., Park, C., Fay, C.C., Wang, X.Q. and Ke, C.H., Appl. Phys. Lett., 2015, 107: 253105
51 Li, L.Y., Li, C.Y. and Ni, C.Y., J. Am. Chem. Soc., 2006, 128: 1692
52 Xu, J.Z., Chen, T., Yang, C L, Li, Z.M., Mao, Y.M., Zeng, B.Q. and Hsiao, B.S., Macromolecules, 2010, 46: 5000
53 Yan, C., Li, H.H., Zhang, J.M., Ozaki, Y., Shen, D.Y., Yan, D.D., Shi, A.C. and Yan, S.K., Macromolecules, 2006, 39: 8041